In-situ Low Power Tests of the ASDEX Upgrade ECRH Transmission Lines

Dietmar Wagner [1*], *Fritz* Leuterer[1], *Francesco* Monaco[1], *Harald* Schütz[1], *Jörg* Stober[1] and *Manfred* Thumm[2]

[1]Max Planck Institute for Plasma Physics, Tokamak Scenario Development, 85748 Garching, Germany
[2]Karlsruhe Institute of Technology, Institute for Pulsed Power and Microwave Technology, 76344 Eggenstein-Leopoldshafen, Germany

Abstract. An Electron Cyclotron Resonance Heating (ECRH) system employing 8 gyrotrons is in routine operation at the ASDEX Upgrade tokamak at IPP Garching. The gyrotrons are of two-frequency type operating at 105 and 140 GHz with a maximum output power of up to 1 MW and 10 s pulse length. The gyrotron output beams are coupled to 8 waveguide transmission lines via quasi-optical Matching Optics Units (MOUs). The oversized corrugated HE11 waveguides with a diameter of 87 mm are operated at atmospheric pressure with overall lengths between 65 and 103 meters. The number of quasi-optical miter bends per line is between 6 and 8. High mode purity in the transmission lines is critical with respect to both, losses and atmospheric breakdowns in the waveguides. Beam measurements at low power have been performed along the transmission lines and are compared to high power measurements. Near-field calculations and measurements of mm-wave beams radiated from open-ended HE11 waveguides show, that varying intensity patterns determine the distribution of Ohmic loading in compact mm-wave beam launching antennas, where the first mirror is located in the reactive near-field or close to the Fresnel maximum.

1 Introduction

The ASDEX Upgrade (AUG) tokamak is equipped with an 8 MW, 105/140 GHz ECRH system employing 8 non-evacuated transmission lines, mainly consisting of corrugated HE11 waveguides (linearly polarized LP01 mode) [1]. The total lengths of the transmission lines are between 65 and 103 meters and the number of miter bends per line is between 6 and 8. The large inner diameter $D = 87$ mm of the corrugated waveguides was chosen in order to avoid atmospheric breakdown at power levels up to 1 MW and to guarantee very low mode-conversion losses at miter bends (around 0.2 % per bend). This is the largest waveguide diameter compared to the wavelength ($40.6 \cdot \lambda_0$ at 140 GHz) of any existing high-power ECRH transmission line [2], where almost 4000 modes (TE and TM) can propagate. While mode conversion in miter bends due to diffraction strongly decreases with increasing D/λ_0 [3], a main concern that led to limitation of waveguide diameters in other systems was coupling to lower order azimuthally asymmetric modes, like the linearly polarized LP_{11}, due to bending of the waveguides caused by sagging or movements of the waveguide supports, abrupt tilts at the waveguide flanges or misalignment of the input millimeter (mm)-wave beam [4]. Low-power measurements at the AUG transmission lines have been performed in search for critical sections of the waveguide transmission line w.r.t. mode conversion. The influence of the coupling between the Matching Optics Unit (MOU) after the gyrotron output and the corrugated waveguide is investigated with thermographic measurements at miter bend mirrors. Near-field measurements of the radiated beam at the open-ended waveguide at low-power have been performed.

2 ASDEX Upgrade ECRH system

The AUG ECRH system includes eight two-frequency GYCOM gyrotrons operating at 105 and 140 GHz [5]. The gyrotons can deliver an output power of up to 1 MW at 140 GHz or slightly reduced power at 105 GHz with a maximum pulse length of 10 s corresponding to the maximum flat top pulse length of the tokamak. All gyrotrons are equipped with depressed collectors and their efficiencies range from 48 % to 54 % at 140 GHz and 46 % and 50 % at 105 GHz. The two-frequency operation of the gyrotrons increases the operating range of the system with respect to the applied magnetic field in the tokamak. Each tube is connected to the Corrugated Waveguide Transmission Line (CWTL) via a quasi-optical MOU (Fig.1). The MOUs contain a set of 2 phase correcting mirrors for each gyrotron frequency followed by a pair of broadband polarizers [6]. A focusing mirror couples the beam to the waveguide. The corrugated HE11 waveguides (*I.D.*= 87 mm) have a design that ensures low-loss transmission of mm-waves over the whole frequency band of the system (Fig.2). A mirror in a shielded box at the end of the transmission line allows for switching of the beam either to another calorimetric load or through a synthetic

* Corresponding author: dietmar.wagner@ipp.mpg.de

diamond vacuum window to the ECRH launcher in the ASDEX Upgrade vacuum vessel. The launcher consists of a fixed focusing mirror followed by a steerable flat mirror allowing for toroidal and poloidal steering of the beam.

Fig. 1. Gyrotron installation at ASDEX Upgrade.

Fig. 2. 87 mm inner-diameter corrugated HE11-mode waveguide transmission lines at ASDEX Upgrade.

3 Low-power measurements at the waveguide transmission line

High power beam measurements at the end of the AUG transmission lines hint at higher order mode contents in the beam (Fig.3). Coupling of a Gaussian beam to a corrugated waveguide with a beam waist at the waveguide entrance of $w_0 = 0.6435 \cdot a$ (a is the waveguide radius) excites about 2 % of spurious modes [4]. These spurious modes are hybrid modes with higher radial indices and all of them have azimuthally symmetric patterns. Therefore, the asymmetric content on the measured beam pattern can either be caused by imperfections of the CWTL (i.e. sagging, tilts or offsets), by imperfect coupling of the free space beam to the waveguide entrance (tilt or offset), or by higher order Gaussian mode content in the free-space beam itself. To separate the influence of the beam coupling from the transmission line, low power tests were performed at the CWTL. A lens horn connected to the input waveguide flange of the transmission line provided a perfect alignment of the input mm-wave beam (Fig.4). The lens horn was optimized to provide a Gaussian beam with $w_0 = 28.0$ mm at the waveguide input. The wave beam along the transmission line was measured at several locations using a mm-wave scanner. A cavity stabilized IMPATT oscillator as source and as receiver a mixer with narrow IF bandwidth (ELVA-1) allowed for measurements with a sensitivity of -60 dBm with no connection between source and receiver. Measurements of the mm-wave beam at arbitrary locations along the transmission line were done by opening of the waveguide line and inserting a miter bend to extract the beam under a 90° angle (Fig.5). Fig.6 shows a comparison between the beam pattern scans of the output of the lens horn and the beam pattern measured after 50 m of waveguide transmission line including 5 miter bends. The scalar Gaussian content of the beam extracted from the waveguide is 98 % compared to 99.7% of the input beam from the lens horn and no asymmetrical beam content was found. Beam pattern were also measured at the end of the transmission line by placing the scanner in the AUG torus (Fig.7). Fig.8 shows the measured output mm-wave beam patterns of transmission lines 3 and 4. There, the beams are radiated from an open-ended waveguide with $D = 130$ mm (following a corrugated taper from $D = 87$ mm to $D = 130$ mm with a length of 1.35 m) via a quasi-optical launcher consisting of a focusing and a flat mirror. The total length of the beam path in free space inside the torus is about 1 m. Both output beams have a scalar Gaussian content of 98 %, which is in good agreement with the theoretical predictions. Again, no asymmetrical spurious mode content was found, proving a good alignment of the waveguide transmission line.

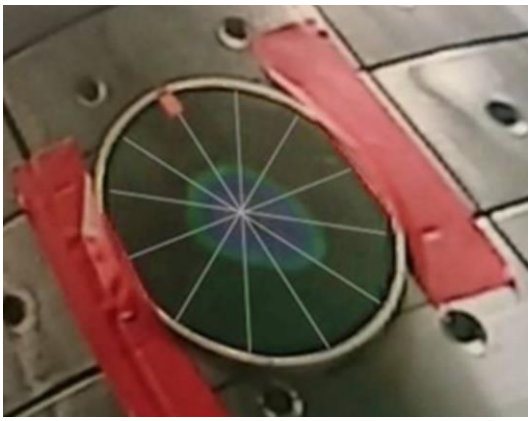

Fig. 3. Hot test with ~1 ms gyrotron pulse at inner torus wall onto a liquid crystal foil target.

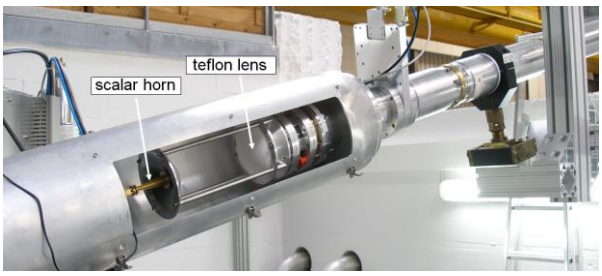

Fig. 4. Lens horn mounted at the input of the corrugated waveguide transmission line for launching the HE11 mode.

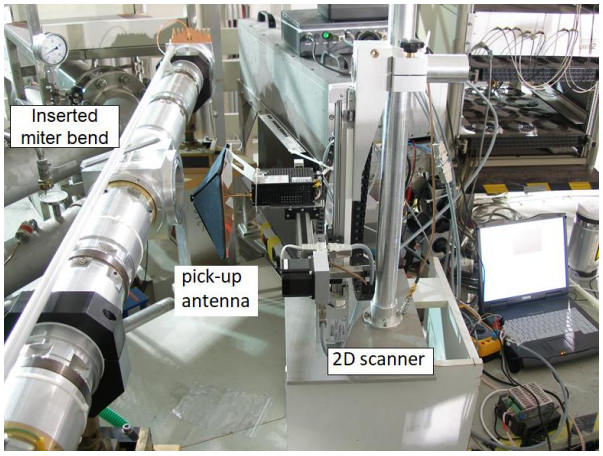

Fig. 5. Scanning of the mm-wave beam along the corrugated waveguide transmission line at the open end of an inserted miter bend.

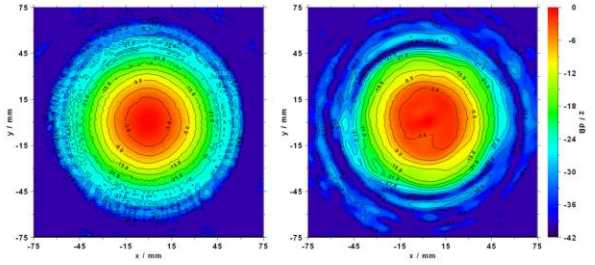

Fig. 6. Measured intensity pattern of the output mm-wave beam of the lens horn (left) and of the extracted beam after 50 m corrugated waveguides including 5 miter bends.

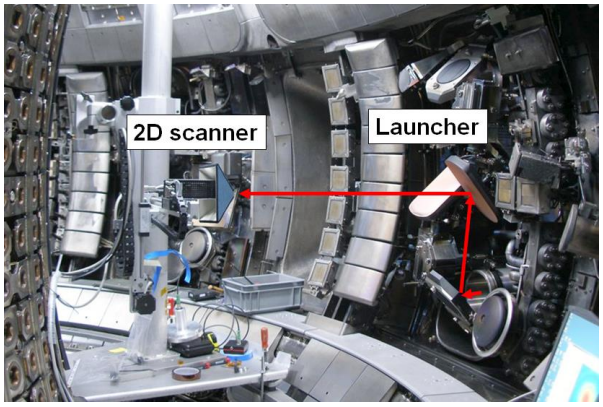

Fig. 7. Measurement of the output mm-wave beam of a AUG transmission line in the torus.

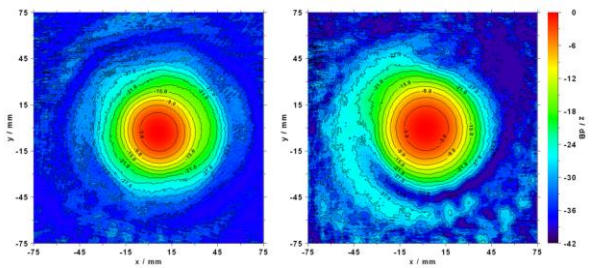

Fig. 8. Beam pattern measured at the end of AUG transmission lines 3 (left) and 4 (right).

4 High-power beam measurements

After confirming a good alignment of the CWTL, the remaining cause for the excitation of asymmetric spurious modes is the coupling of the high-power beam to the CWTL via the MOU, or the beam quality itself.

4.1 Alignment of the Matching Optics Unit

Fig. 9 shows the mirror setup in the MOU. The gyrotron beam is directed onto a pair of phase correcting mirrors. These are mounted on turntables to provide a set of two of phase correcting mirrors for each frequency (105 and 140 GHz). These mirrors are followed by two broadband polarizers [6]. The last mirror focuses the beam to the entrance of the CWTL. Additional mirrors can be flipped into the beam path to direct the beam into a 1 MW, 1s load, used for gyrotron conditioning, which is also part of each MOU. Alternatively the beam can be switched to a long pulse load (1 MW, 10s) or a short pulse (200 ms) calorimetric load. The first part of the alignment is purely optical using a laser mounted in the open-ended waveguide entrance of the CWTL. Using small optical mirrors glued to the center of the MOU mirrors, the mirrors are aligned with the waveguide axis in reverse direction up to the second phase correcting mirror M2. The task is then to align the gyrotron output beams at both frequencies with this optical beam axis. This is done in a second step using the two phase-correcting mirrors M1 and M2. These mirrors can be tilted in two directions, both along the MOU mm-wave beam path and perpendicular to it. They can also be slightly shifted on their supports. The alignment is checked with short high-power pulses (0.5-1 ms) onto temperature-sensitive liquid crystal foils which are placed on each mirror and also at the CWTL entrance. The measured patterns are compared with the theoretical power distributions on the mirrors as obtained during the mirror synthesis [7]. The measured pattern can be compared with theoretical power distributions on the mirrors in order to correct the tilt angles of the two phase-correcting mirrors. Some examples of such measured beam patterns are shown in Fig.10.

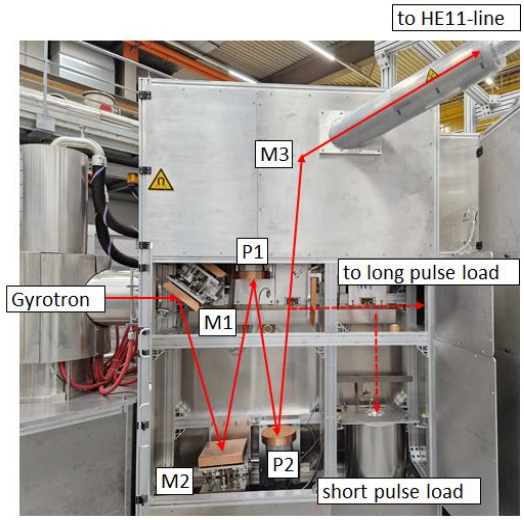

Fig. 9. Matching Optics Unit (MOU) with phase correcting mirrors M1 and M2, followed by the polarizers P1 and P2 and a focusing mirror M3 (not visible in this picture).

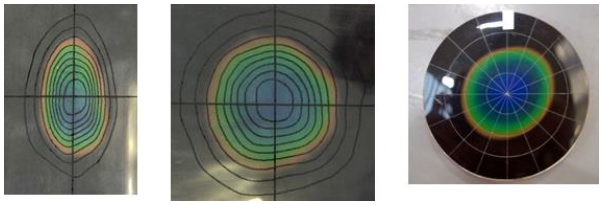

Fig. 10. Measured high-power mm-wave beam pattern at the first (left) and second (middle) phase correcting mirrors and at the waveguide entrance (right).

4.2 Beam pattern measurements at miter bends

Additional measurements along the CWTL are necessary to verify the alignment of the high-power beam w.r.t. the waveguide axis. In order to allow for high power in-situ measurements without opening of the CWTL, a thermographic miter bend detector has been developed (Fig.11). For this, the miter bend copper mirror is replaced with a thin (0.5 mm) stainless steel mirror. The outside surface of the mirror is coated with a thin layer of zinc paint that provides good IR emissivity and low IR reflectivity while having a good heat resistivity at the same time. The detector allows for gyrotron pulse lengths up to 60 ms compared to the very short pulse lengths applied for measurements with the liquid crystal foils which might be still influenced by the frequency chirp at the beginning of the gyrotron pulse. Fig.12 shows the measurement setup with the miter bend IR detector mounted at the first miter bend of AUG CWTL #3. In Fig.13, the measured temperature distribution at this miter bend is plotted. The pattern shows a clear asymmetry, although the input beam was previously aligned to the entrance of the CWTL as described in the previous chapter, using liquid crystal foils, hinting at a slight misalignment w.r.t. the waveguide axis. By tilting the second phase correcting mirror by only 0.032 deg. in the plane perpendicular to the MOU axis a more symmetric temperature distribution on the miter bend mirror could be achieved (Fig.14). In order to get unambiguous results with respect to the symmetry of the beam, at least 3 measurements at different distances are required to cope for eventual beating structures of the HE_{11} mode with spurious modes. This is work in progress which could potentially further improve the alignment of the gyrotron beam with the CWTL.

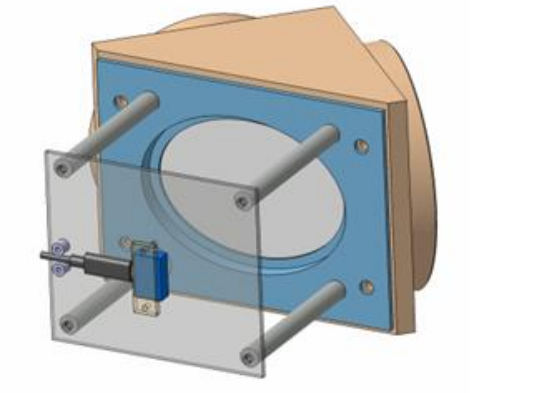

Fig. 11. Drawing of miter bend IR detector with a thin outside coated stainless steel mirror and mounted IR camera.

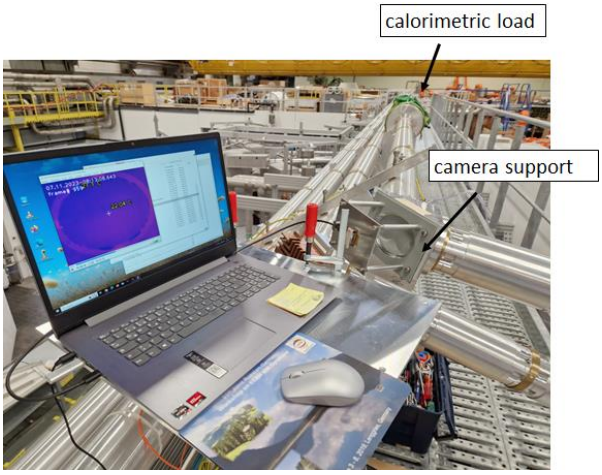

Fig. 12. Miter bend IR detector mounted at the first miter bend of an AUG CWTL.

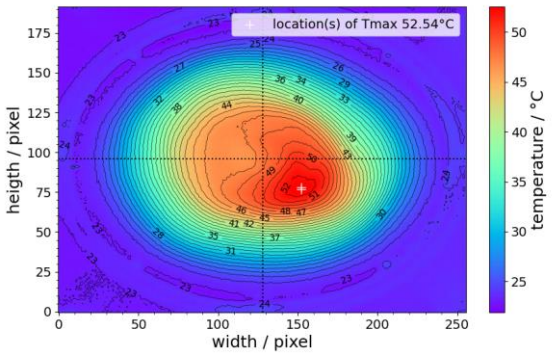

Fig. 13. Measured temperature distribution at the first miter bend of AUG CWTL #3.

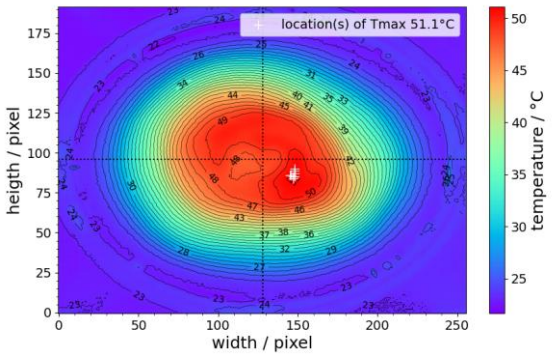

Fig. 14. Measured temperature distribution at the first miter bend of AUG CWTL #3 after tilting the second phase correcting mirror by 0.032 deg. Perpendicular to the MOU axis.

5 Near-field low-power measurements

Near field effects when radiating from an open-ended corrugated waveguide due to interference with spherical waves which are excited at the waveguide truncation are expected [8]. The far field region for the AUG waveguides with a diameter of 87 mm only begins at a distance of about z = 7 m = $2 \cdot D^2/\lambda_0$. This means that most optical components connected to the AUG CWTL are mounted in the near field region. The calculated

field intensity on the waveguide axis of a radiated HE11 mode as a function of the distance from the open-ended waveguide in the near field region was calculated with a mode matching code and compared to the values resulting from the field approximation of a Gaussian beam (Fig.15). The reactive near field with oscillating intensity along the axis ends with the minimum at approximately z = 350 mm, which very well corresponds to [9]:

$$z = 0.62\sqrt{D^3/\lambda_0}. \quad (1)$$

The power maximum in the following radiating near-field (Fresnel) region, the Fresnel maximum [10], is located at z = 630 mm. To measure these near-field effects the lens horn was connected to pieces of corrugated waveguide of different lengths (0.5, 1.0 and 1.5 m) and mounted on a rail together with the scanner to provide good alignment (Fig.16). Then the near-field intensity was measured at different distances from the open-ended corrugated waveguide and compared to calculations assuming a Gaussian beam with w_0 = 28.0 mm coupled to the corrugated waveguide with a diameter of D = 87 mm. The measurements are in good agreement with the calculations (Fig.17). The differences in the measurements for different lengths of waveguides can be explained by the imperfect coupling of the Gaussian free-space beam to the HE11 corrugated waveguide eigenmode. The beat wavelength of the main spurious mode (HE12) with the HE11 mode is 2.2 m. Depending on the phase difference between the HE11 and spurious modes, this will cause a variation of the aperture field at the open end of the waveguide and therefore a difference in the field intensity along the longitudinal axis.

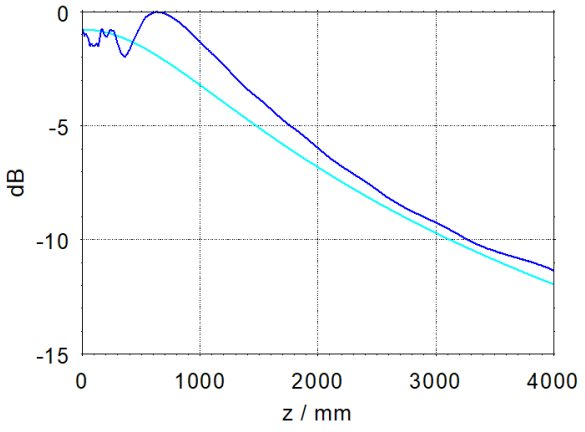

Fig. 15. Calculated relative intensity on the waveguide axis for an HE11 mode radiated from an open-ended corrugated waveguide with D = 87 mm at f = 140 GHz (dark blue) compared to a Gaussian field approximation (light blue). Since the Fourier transform (far field) of a Gaussian aperture field distribution is a Gaussian function again, there are no near-field effects in this case.

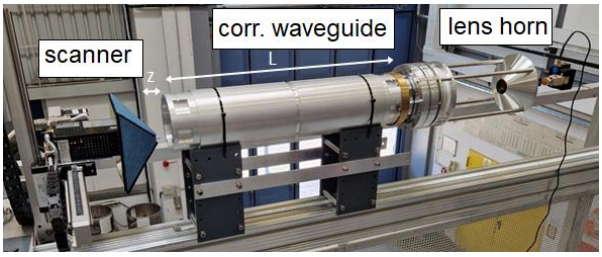

Fig. 16. Measurement setup for near-field measurements.

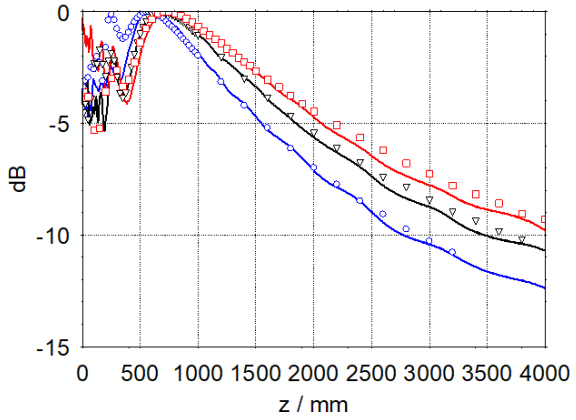

Fig. 17. Comparison between measured (dots) and calculated (solid lines) relative field intensity as a function of the distance from the open-ended corrugated waveguide for different waveguide lengths (red: 0.5 m, black: 1.0 m and blue: 1.5 m)

Calculations for less oversized corrugated HE11 waveguides give similar near-field intensity distributions. Figs. 18-20 give the relative field intensity for an HE11 mode radiated from the open-ended waveguides applied for the DIII-D ECH system (D = 31.75 mm, f = 110 GHz) [11], the waveguides foreseen for Collective Thomson Scattering (CTS) diagnostic on ITER (D = 88.9 mm, f = 60 GHz) [12] and the waveguides planned for the ITER ECRH system (D = 50.0 mm, f = 170 GHz) [13]. The measurements with the ASDEX Upgrade waveguides and all the calculations presented here, show that the location of the field intensity maximum (Fresnel maximum) is at approximately:

$$z = 0.7 \cdot D^2/4\lambda_0. \quad (2)$$

A simulation of the two-dimensional field intensity distribution of the HE11 mode radiated from a waveguide with D = 31.75 mm at 110 GHz is given in Fig.21 and the mm-wave beam pattern in the plane of the Fresnel maximum is plotted in Fig.22, which clearly shows the peaking of the field intensity.

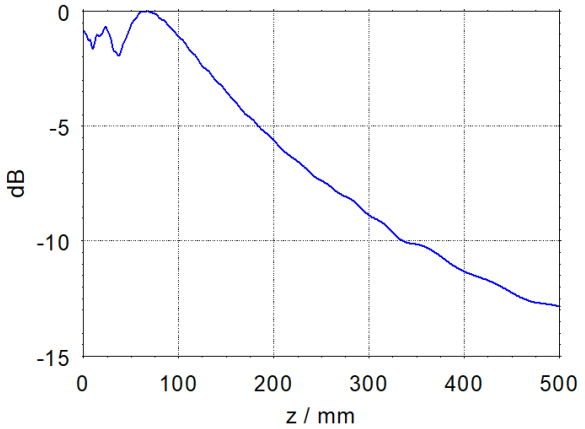

Fig. 18. Calculated relative intensity on the waveguide axis for the HE11 mode radiated from an open-ended corrugated waveguide with D = 31.75 mm at f = 110 GHz.

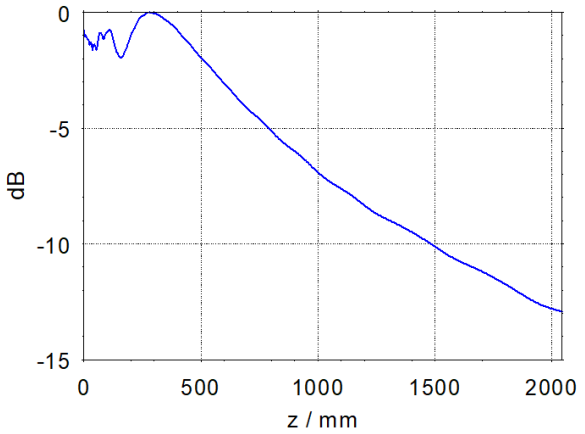

Fig. 19. Calculated relative intensity on the waveguide axis for the HE11 mode radiated from an open-ended corrugated waveguide with D = 88.9 mm at f = 60 GHz.

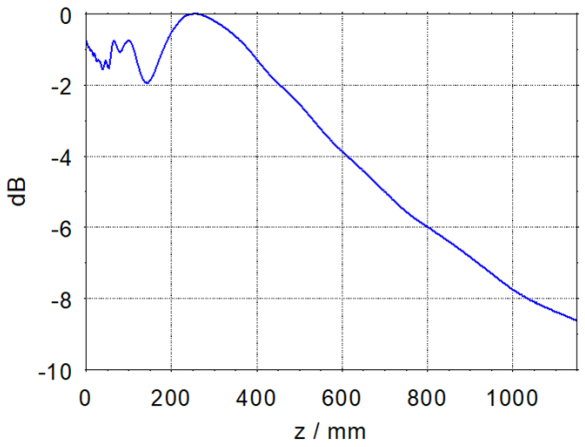

Fig. 20. Calculated relative intensity on the waveguide axis for the HE11 mode radiated from an open-ended corrugated waveguide with D = 50.0 mm at f = 170 GHz.

This on-axis intensity peaking by approx. a factor of 1.6 compared to a Gaussian distribution (see Fig.15) has to be considered in the calculation of the distribution of Ohmic mirror loading in compact, quasi-optical mm-wave beam launching antennas of ECRH and CTS systems, where the first mirror is located close to the Fresnel maximum.

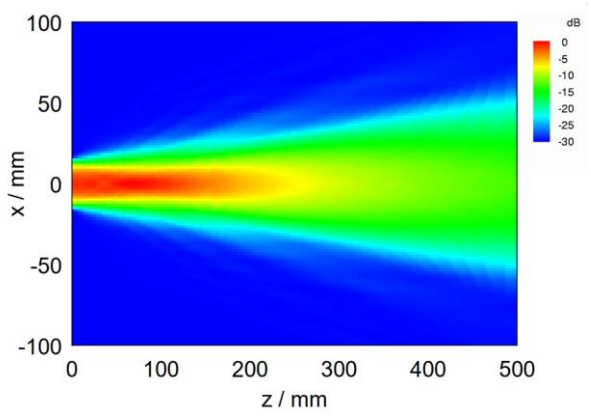

Fig. 21. Calculated field intensity distribution of the HE11 mode radiated from an open-ended corrugated waveguide with D = 31.75 mm at f = 110 GHz.

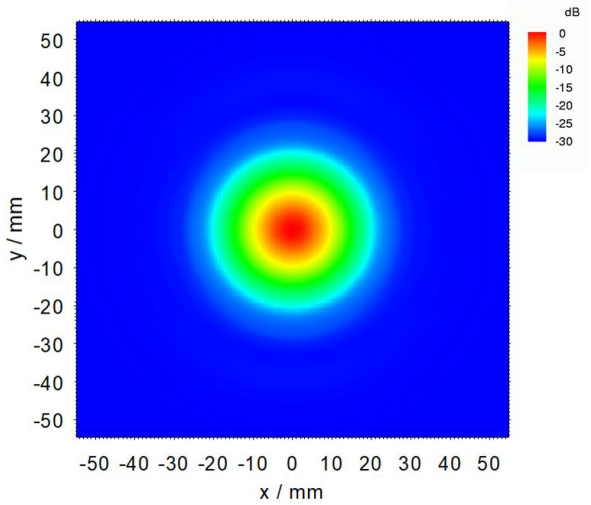

Fig. 22. Calculated field intensity distribution of the HE11 mode radiated from an open-ended corrugated waveguide with D = 31.75 mm at f = 110 GHz at z = 66 mm (Fresnel maximum).

6 Conclusions

Cold tests with a lens horn at ASDEX Upgrade transmission lines at different locations along the waveguide path have been performed and revealed a good alignment of the transmission lines. No indication of parasitic mode excitation due to sagging or tilts of the waveguides has been found. A comparison with high-power beam measurements indicated that the coupling of the free-space beam from the MOU to the corrugated HE11-mode waveguide transmission line is critical for spurious mode excitation. A new high-power beam detection system at miter bends is presented which potentially allows for a more precise alignment of the free-space beam to the waveguide transmission line. Near field calculations and measurements of mm-wave beams radiated from the open-ended waveguide show an intensity focus (Fresnel maximum) at a distance from the open-ended waveguide that depends on both, the waveguide diameter and the frequency. This intensity peaking compared to a Gaussian distribution has to be

considered in the simulation of the distribution of Ohmic loading in compact, mm-wave beam launching antennas, where the first mirror is located in a plane near the Fresnel maximum. The influence of the slight mismatch in the coupling of a Gaussian free-space beam to the HE11 mode at the input of the CWTL on the output beam radiated from the open-ended waveguide is shown.

References

1. J. Stober et al., Exploring fusion-reactor physics with high-power electron cyclotron resonance heating on ASDEX Upgrade, Plasma Phys. Control. Fusion **62**, 024012 (2020), DOI 10.1088/1361-6587/ab512b
2. H. Yamazaki et al., Evaluation of transmission efficiency of the ECH/CD transmission lines in integrated commissioning phase on JT-60SA, Fusion Engineering and Design **196**, 114015 (2023), DOI 10.1016/j.fusengdes.2023.114015.
3. J. L. Doane, Design of circular corrugated waveguides to transmit millimeter waves at ITER, Fusion Sci. Technol. **53**, No. 1, 159–173 (2008) DOI api.semanticscholar.org/ CorpusID:116784734
4. E. J. Kowalski et al., Linearly polarized modes of a corrugated metallic waveguide, IEEE Transactions on Microwave Theory and Techniques **58**, No. 11, 2772-2780 (2010), DOI 10.1109/TMTT.2010.2078972
5. Zapevalov et al., Development of a prototype of a 1-MW 105-156-GHz multifrequency gyrotron. Radiophysics and Quantum Electronics **47**, No. 5-6, 396–404 (2004). DOI 10.1023/B:RAQE.0000046313. 84364.3c
6. D. Wagner and F. Leuterer, Broadband polarizers for high-power multi-frequency ECRH systems, Int J Infrared and Milli Waves **26**, No. 2, 163-172 (2005), DOI 10.1007/s10762-005-2997-x
7. A. Chirkov et al., 3D wavebeam field reconstruction from intensity measurements in a few cross sections, Optics Communications **115**, 449-452 (1995), DOI 10.1016/0030-4018(94)00630-D
8. R. Cicchetti and A. Faraone, Radiation from open-ended circular waveguides: a formulation based on the incomplete Hankel functions, Progress In Electromagnetics Research **78**, 285-300 (2008), DOI 10.2528/ PIER07091405
9. C. A. Balanis, Antenna Theory: Analysis and Design, 3rd ed., p. 34, Wiley-Interscience, John Wiley & Sons Inc. (2005), ISBN: 0-471-66782-X
10. Arnold Sommerfeld, Vorlesungen über Theoretische Physik, Band IV, Optik, 3. Auflage, pp. 187-189, Akademische Verlagsgesellschaft, Leipzig 1964.
11. I.A. Gorelov et al., ECH system on the DIII-D tokamak, Proc. 15th Joint Workshop on Electron Cyclotron Emission and Electron Cyclotron Resonance Heating (EC-15), ed. J. Lohr, pp. 446-451 (2008), World Scientific, DOI 10.1142/9789812814647_0063
12. S.B. Korsholm et al., Design and development of the ITER CTS diagnostic, Electron Cyclotron Emission and Electron Cyclotron Resonance Heating (EC-20), EPJ Web of Conferences **203**, 03002 (2019), DOI 10.1051/epjconf/ 201920303002
13. T.P. Goodman et al. High-power testing of guided-wave components for the ITER ECH Upper Launcher at the FALCON Test Facility, IEEE Transactions on Plasma Science **48**, No. 6, 1537-1542 (2020), DOI 10.1109/TPS.2019.2945126